Particle shape effects on thermophysical properties of alumina nanofluids

Elena V. Timofeeva,[1,a)] Jules L. Routbort,[1] and Dileep Singh[2]
[1]*Energy Systems Division, Argonne National Laboratory, Argonne, Illinois 60439, USA*
[2]*Nuclear Engineering Division, Argonne National Laboratory, Argonne, Illinois 60439, USA*

(Received 14 January 2009; accepted 25 May 2009; published online 6 July 2009)

The thermal conductivity and viscosity of various shapes of alumina nanoparticles in a fluid consisting of equal volumes of ethylene glycol and water were investigated. Experimental data were analyzed and accompanied by theoretical modeling. Enhancements in the effective thermal conductivities due to particle shape effects expected from Hamilton–Crosser equation are strongly diminished by interfacial effects proportional to the total surface area of nanoparticles. On the other hand, the presence of nanoparticles and small volume fractions of agglomerates with high aspect ratios strongly increases viscosity of suspensions due to structural constrains. Nanoparticle surface charge also plays an important role in viscosity. It is demonstrated that by adjusting *p*H of nanofluid, it is possible to reduce viscosity of alumina nanofluid without significantly affecting thermal conductivity. Efficiency of nanofluids (ratio of thermal conductivity and viscosity increase) for real-life cooling applications is evaluated in both the laminar and turbulent flow regimes using the experimental values of thermal conductivity and viscosity. © *2009 American Institute of Physics*. [DOI: 10.1063/1.3155999]

I. INTRODUCTION

The thermal conductivity of heating/cooling fluids plays a vital role in the development of energy efficient heat transfer equipment for electronics, transportation, energy supply, and production. However, conventional heat transfer fluids such as 50/50 mixture of ethylene glycol and water (EG/H_2O) have poor thermal conductivities compared to most solids. In nanofluids (solid nanoparticles dispersed in liquids) high thermal conductivities of solid nanoparticles effectively increase the thermal conductivity of the suspensions. Considerable research in last decade has been devoted to the study of steady-state thermal conductivity of nanomaterial suspensions[1–3] and measured high thermal conductivities were used to imply enhanced energy transport capabilities of nanofluids.

However, in most practical applications[4] the heat transfer fluids are not stationary and the convective heat transfer coefficient becomes important. Calculation of the heat transfer coefficient of the coolant and pressure drop in the heat exchanger or the radiator includes four basic thermophysical properties, i.e., viscosity, density, specific heat, and thermal conductivity. Introduction of nanoparticles to the fluid not only enhances thermal conductivity but, unfortunately, often causes significant increase in viscosity.[5,6] The latter effect is undesirable and might raise the questions about effectiveness of the nanofluid as a coolant. Any gain in heat transfer and hence reduction in radiator size and weight could be compromised by increased pumping power.

Therefore development of a heat transfer nanofluid requires a complex approach that accounts for changes in all important thermophysical properties caused by introduction of nanomaterials to the fluid and not just the thermal conductivity value. Thus, the challenge of nanofluid development is in understanding of how micro- and macroscale interactions between particles and fluid affect thermophysical properties of suspension. It is obvious that these correlations depend on many factors, i.e., material of nanoparticles, concentration, size and shape, properties of the base fluid, and the presence of other substances, surfactants, electrolyte strength, and *p*H.

In this investigation, we studied the effect of nanoparticle shape on viscosity and thermal conductivity for 50/50 EG/H_2O based suspensions of alumina nanoparticles. We have correlated experimental data with nanoparticle morphologies and the existing theories for thermal conductivity and viscosity of suspensions, accounting for the complexity of nanofluid system and potential contributions to the thermophysical properties. Finally, cooling efficiencies of resulting nanofluids were evaluated for laminar and turbulent flow modes.

II. THEORETICAL BACKGROUND

Reliable universal theoretical models for prediction of the thermal conductivity of nanoparticle suspensions have not been developed despite extensive research. The macroscopic effective medium theory (EMT) introduced by Maxwell[7] and further developed for nonspherical particle shapes by Hamilton and Crosser[8] predicts that thermal conductivity of two component heterogeneous mixtures is a function of the conductivity of pure materials, the composition of the mixture, and the manner in which pure materials distributed throughout the mixture. Hamilton–Crosser model allows calculation of the effective thermal conductivity (k_{eff}) of two component heterogeneous mixtures and includes empirical shape factor n given by $n=3/\psi$ (ψ is the sphericity defined as ratio between the surface area of the sphere and the surface area of the real particle with equal volumes),

[a)]Author to whom correspondence should be addressed. Electronic mail: etimofeeva@anl.gov.

 © 2009 American Institute of Physics

Downloaded 06 Jul 2009 to 146.139.240.6. Redistribution subject to AIP license or copyright; see http://jap.aip.org/jap/copyright.jsp

$$\frac{k_{\text{eff}}}{k_0} = \frac{k_p + (n-1)k_0 + (n-1)(k_p - k_0)\phi}{k_p + (n-1)k_0 - (k_p - k_0)\phi}, \quad (1)$$

where k_p and k_0 are the conductivities of the particle material and the base fluid and ϕ is volume fraction of nanoparticles. Thus, according to this model,[8] suspensions of particles with high shape factor (elongated and thin) should have higher thermal conductivities, if the ratio of conductivities of two phases is above 100.

Despite the large database supporting EMT, there are many experimental results showing significantly higher or lower thermal conductivity enhancements,[1–3] indicating that basic EMT does not account for all contributing factors. A number of mechanisms for enhancing thermal conductivity were suggested to explain the experimental data, including the interaction between nanoparticles and liquids, interfacial resistance,[9–11] formation of nanolayers,[12,13] the size[14] and agglomeration of nanoparticles,[15,16] and finally the heat convection due to Brownian motion of nanoparticles in the liquid (microconvection).[17–19] However, none of these mechanisms alone seems to be able to explain the thermal conductivity enhancements in various nanofluids.

Lately several research groups agreed that (at least for metal oxide suspensions) temperature contributions inherent in Brownian motion models are not necessary to describe the temperature dependence of the thermal conductivity of nanofluids.[20–22] It was shown[21] that the microconvection model overestimates the thermal conductivity with nonphysical dependence on the nanoparticle density, while the effect of mass or volume fraction of nanoparticles can be corrected using EMT based models[20] with one adjustable parameter (the shape factor or ordered liquid layer thickness).

Interactions between the nanoparticles and the fluid are manifested through the interfacial resistance that arises because interfaces act as an obstacle to heat flow and diminish overall thermal conductivity of the system. For phonon-based conductors, the interfacial thermal resistance, also known as Kapitza resistance (R_k), may arise from phonon scattering at the interface. A more transparent definition can be obtained by defining the Kapitza length,

$$l_k = R_k k_0, \quad (2)$$

where k_0 is the thermal conductivity of the matrix and l_k is simply the thickness of base fluid equivalent to the interface from a thermal point of view (excluded from thermal transport).[11]

The values of Kapitza resistance (or length) can be extracted from equilibrium or nonequilibrium molecular dynamic simulations.[11,23] They were shown to depend on the strength of solid-liquid interaction. In composite systems such as nanofluids, contribution of interfacial properties to macroscopic thermal conductivity measurement should be significant and depend not only on the value of surface resistance but also should be proportional to the total surface area of particles in nanofluids.

Rheological properties are strongly related to the nanofluid's microstructure. The nanoparticles suspended in a base fluid are in random motion under the influence of several acting forces such as Brownian motion (Langevin force, that is random function of time and reflects the atomic structure of medium), viscous resistance (Stokes drag force), intermolecular van der Waals interaction (repulsion, polarization, and dispersion forces), and electrostatic (Coulomb) interactions between ions and dipoles. Nanoparticles in suspension can be well dispersed (particles move independently) or agglomerated (ensembles of particles move together). Depending on the particle concentration and the magnitude of particle-particle interaction that are affected by *p*H, surfactant additives, and particle size and shape,[24] an dispersion/agglomeration equilibrium establishes in nanoparticle suspension. It should be noted here that two types of agglomerates are possible in nanofluids. First type of agglomerates occurs when nanoparticles are agglomerated in dry powders (polycrystalline nanoparticles). Those agglomerates are unlikely to be broken apart when nanoparticles are suspended into the fluid and potentially can provide increased thermal conductivity as described by Prasher *et al.*[16] When loose single crystalline nanoparticles are suspended, each particle acquires diffuse layer of fluid intermediating particle-particle interactions in nanofluid. Due to weak repulsion such nanoparticles can form aggregate-like ensembles moving together, but in this case interfacial resistance at solid/liquid/solid interface is likely to prevent proposed enhancement in thermal conductivity due to agglomeration effect.[16]

Agglomeration and clustering of nanoparticles result in undesirable viscosity increase. Einstein–Batchelor equation[25] describes the dependence of viscosity increase with concentration of particles in the simplest case of dilute suspensions ($\phi < 0.10$) of uncharged, hard, noninteracting spherical particles,

$$\eta_{\text{eff}} = \eta_0(1 + 2.5\phi + 6.2\phi^2), \quad (3)$$

where η_0 is viscosity of base fluid. This equation will be used as a baseline for our study of nanofluid viscosity.

Functional dependence of the viscosity on the fluid temperature can be expressed by Arrhenius-type equation,[26]

$$\eta_{\text{eff}} = \eta_{\infty,T} e^{E_a/(\text{RT})}, \quad (4)$$

where η_{eff} is the viscosity from experimental tests, $\eta_{\infty,T}$ is the viscosity at "infinite temperature," E_a is the activation energy to fluid flow, R is the universal gas constant, and T is the temperature in kelvins. The activation energy E_a and infinite-temperature viscosity $\eta_{\infty,T}$ are parameters that reflect the behavior of fluids and can be extracted from experimental data through the logarithmic form of the Arrhenius equation.

III. MATERIALS AND METHODS

The nanoparticles of different shapes used in this work were boehmite alumina supplied by Sasol North America Inc. Particle shapes and nominal sizes provided by the manufacturer were determined from transmission electron microscopy (TEM) images and are summarized in Table I. Nanopowders were independently characterized by x-ray diffraction (XRD) performed on a Philips X'PERT powder diffractometer with a Cu $K\alpha$ x-ray source. Manufacturer reported that provided nanopowders have different admixtures

Downloaded 06 Jul 2009 to 146.139.240.6. Redistribution subject to AIP license or copyright; see http://jap.aip.org/jap/copyright.jsp

TABLE I. Morphology of alumina nanopowders and EG/H_2O based nanofluids (TEM images and designations provided by manufacturer).

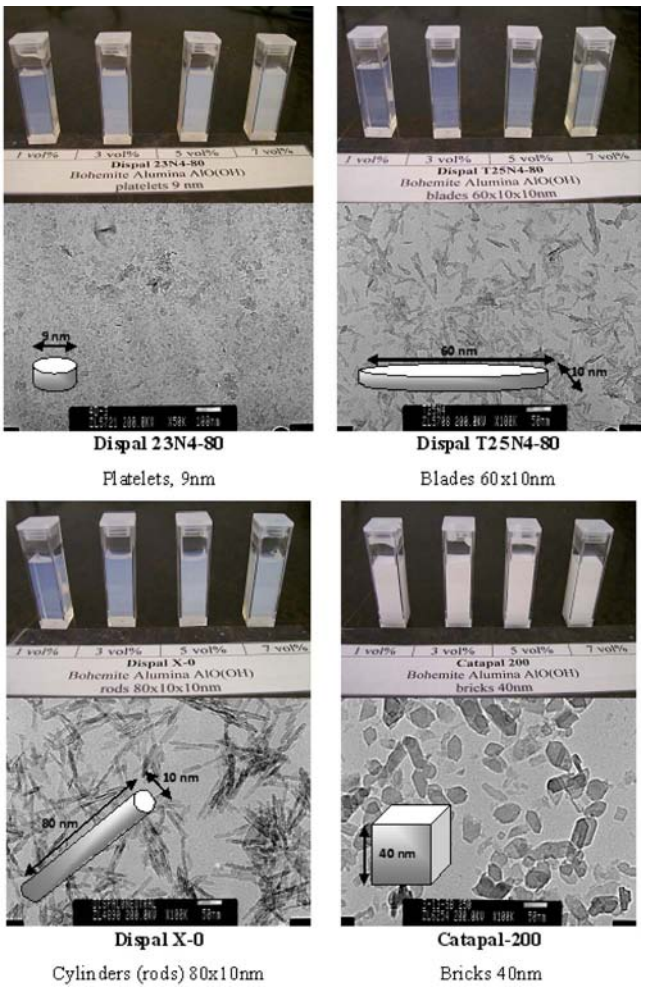

of monovalent acids (nitric, acetic, or formic), typically <2 wt % of dry powders for better dispersibility in fluids. Those acids do not adsorb specifically on alumina surfaces and dissolve readily when alumina is dispersed in water. Therefore, the presence of admixtures may affect the *p*H of suspension, stability, and agglomeration of nanoparticles.

The same batch of deionized water and laboratory grade EG 99+% (Fisher) mixed 50/50 by volume was used as the base fluid for all preparations. The volume fraction (vol %) of the nanopowders was first estimated from the weight of dry powder using the true density of boehmite alumina (AlOOH, 3.05 g/cm^2) (Ref. 27) and the total volume of suspension. Suspensions with 1.0–8.4 vol % of solid nanoparticles were prepared. Nanoparticles were dispersed in the base fluid and continuously mixed using magnetic stirrer for 3 days. During this time the mixture was also sonicated (three to five sessions for 15 min) with a Branson Sonicator 450 in pulsed regime (40%–60% of second) and 150–200 W output power. Minor sediments were observed a week after nanofluid preparation. They were decanted, dried, and weighted. It was shown that less than 3% of total nanopowders added to the base fluids settle after preparation (maximum concentrations change of 0.2 vol %). Remaining fluids appeared stable as no sedimentation was observed over a 3 month period (balance of gravitational and thermal energy of particles prevents them from settling). Measuring the density of suspension provided additional control of volume fraction. Correction for the sedimentation to the volume percentage was applied prior to the data interpretation.

Nanofluids *p*H were measured with a ExStik *p*H(PH100) meter manufactured by ExTech instruments. Solution of $2N$ HNO_3 in EG/H_2O mixture was used for *p*H adjustments. Agglomeration and the particle size distribution in diluted [$\sim$0.01 vol %, limitation of dynamic light scattering (DLS), and small angle x-ray scattering (SAXS) techniques to dilute solutions arise because of multiple scattering in concentrated suspensions] nanofluids were studied with the DLS technique at a 90° scattering angle, on a 90Plus/BI-MAS particle size analyzer from Brookhaven Instruments Corp.

The nanofluid effective thermal conductivity was measured using a thermal property analyzer (model KD2pro, Decagon Devices, Inc.) based on the transient hot wire method.[28] Small temperature rises ($\sim$0.5 °C) were applied to eliminate errors that could arise due to temperature induced fluid convection. To avoid convection due to external vibrations, sample vial (90×27 mm; length$\times$diameter) with the probe inside (60×1.3 mm) was mounted in a massive metal stand inside of the styrofoam container placed on the marble table in the building basement. Because of small temperature gradients used in the measurement, the probe was found to be very sensitive to minor changes (±0.1 °C) in room temperature, especially for fluids with low viscosities. Random errors were eliminated by using an average of over hundred measurements taken automatically every 15 min. The standard deviation was typically less than 2% at 21 ± 0.5 °C. The accuracy of the probe and the approach to

TABLE II. Characterization of particle sizes in alumina powders and EG/H_2O based suspensions.

Nanoparticles	Platelets	Blades	Cylinders	Bricks
Manufacturer description	9 nm	60×10 nm	80×10 nm	40 nm
XRD, crystallite sizes (spheres)	8.6 ± 2.2 nm	7.7 ± 1.5 nm	14.2 ± 2.2 nm	31.7 ± 2.6 nm
DLS (diluted suspension)	13.4 nm (87 vol %)	9.5 nm (56 vol %)	22–50 nm (93 vol %)	49–78 nm (75 vol %)
	67 nm (12 vol %)	28–52 nm ($\sim$40 vol %)	148–162 nm (<5 vol %)	220–250 nm (<25 vol %)
	$\sim$200 nm (<1 vol %)	300–400 nm (<2 vol %)		
SAXS (diluted suspension)	Aspect ratio: 0.15	Aspect ratio: 6	Aspect ratio: 8	19–47 nm (major) 76–96 nm
	dimensions $16\times16\times3$ nm	dimensions $36\times6\times6$ nm	dimensions $64\times8\times8$ nm	Mean diameter of 54 nm.

Downloaded 06 Jul 2009 to 146.139.240.6. Redistribution subject to AIP license or copyright; see http://jap.aip.org/jap/copyright.jsp

data collection was carefully checked on pure water and EG and was found to be in good agreement with literature values of the thermal conductivity of those fluids.

The relative viscosity of alumina nanofluids was measured using a Brookfield DV-II+ rotational-type viscometer with the SC4–18 spindle. Flow behavior of nanofluids was tested at various share rates (39.6–264 1/s) and temperatures (15 to 85 °C ± .2 °C). For all reported viscosity data >10% torque criterion was satisfied.

IV. RESULTS

A. Particle sizes and distributions

XRD patterns obtained from the alumina nanopowders used for the nanofluid preparation match the spectra of the boehmite phase of alumina. The crystallite sizes of alumina samples calculated from XRD peak broadening by the Debye–Scherer equation[29] (assuming spherical particles) are presented in Table II. Estimated crystallite sizes are close to particle sizes quoted by manufacturer. Thus, we conclude that alumina nanopowders under study are composed of the same phase and mostly are single crystallites. This fact is important for modeling and comparison of nanofluid properties.

Average sizes of dispersed alumina nanoparticles in diluted nanofluids were characterized using DLS. Smallest particle sizes seen by DLS are close to the size of nanopowder crystallites, determined from XRD (Table II). Volume content of each particle size can be approximated from multimodal size distribution. One can see from Table II that agglomeration in most of studied nanofluids is minimal, platelets suspension have less than 1 vol % of agglomerates, blades less than 2 vol %, cylinders less than 5 vol %. Suspension of bricklike particles showed less than 25% of agglomerates which are not larger than four to six particle diameters. Even though there may be some formation of agglomerates, the contribution to thermal conductivity will be minimal because of thermal resistance at solid/liquid/solid interface which is likely to prevent the effect of aggregates proposed by Pracher.[16]

Another technique we used for determination of particle size distribution in suspensions is SAXS. This technique uses x-rays and is sensitive to the change in electronic density around the particle.[30] Detailed results on the particle size distribution from all techniques are summarized in Table II and used later for modeling of nanofluid behavior.

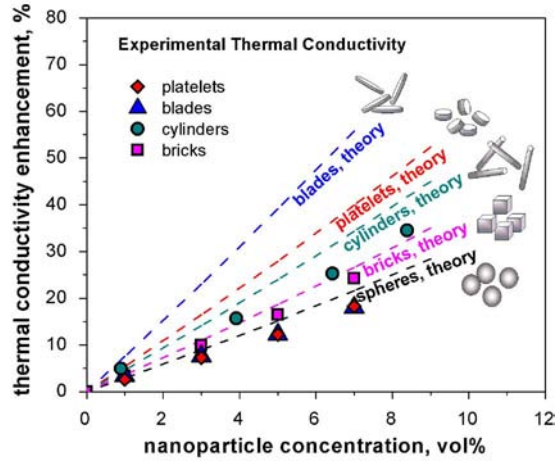

FIG. 1. (Color online) Experimentally measured thermal conductivity of alumina nanofluids in EG/H_2O compared to predictions of Hamilton–Crosser model for corresponding particle shapes.

B. Thermal conductivity

The thermal conductivities of alumina nanofluids (k_{eff}) with different particle shapes measured at room temperature (21 ± 0.5 °C) are presented in Fig. 1 as a function of nanoparticle volume fraction. The thermal conductivity enhancement is defined as k_{eff}/k_0 ratio (expressed as a percent enhancement on graphs) where k_0 is the thermal conductivity of the base liquid (50/50 EG/H_2O). At tested particle concentrations thermal conductivity of nanofluids linearly increases with increase in nanoparticle volume fraction ( ). This type of linear dependence can be written as

$$k_{eff}/k_0 = 1 + C_k \quad , \tag{5}$$

where C_k is thermal conductivity enhancement coefficient. C_k is independent of volume fraction and normalized to the thermal conductivity of base fluid.

Thus the thermal conductivity increase in alumina nanofluids with different particle shapes can be evaluated by the experimental thermal conductivity enhancement coefficients (C_k) which are presented in Table III and follow the sequence (from low to high): platelets (Dispal 23N4-80) ≈blades (Dispal T25N4-80)<bricks(Catapal 200)<cylinders(Dispal X-0), indicative of the effect of particle shape on thermal conductivity which will be addressed in Sec. V.

C. Viscosity

Viscosity of nanofluids ($_{eff}$) as a function of nanoparticle volume fraction, measured at constant share rate and temperature of 25 °C, are presented in Fig. 2. It can be seen

TABLE III. Contribution of particle shape effect and surface resistance to thermal conductivity of nanoparticle suspensions.

	Aspect ratio	Sphericity ψ	Shape factor $n=3/\psi$	C_k	C_k^{shape}	$C_k^{surface}=C_k-C_k^{shape}$	Surface factor f (1/nm)	Kapitza length l_k (nm)	Kapitza resistance R_k (m^2 K/W)
Platelets	1:1/8	0.52	5.7	2.61	5.72	−3.11	2.22	1.44	3.8×10^{-9}
Blades	1:6:1/12	0.36	8.6	2.74	8.26	−5.52	3.29	1.59	4.2×10^{-9}
Cylinders	1:8	0.62	4.9	3.95	4.82	−0.87	0.58	1.79	4.7×10^{-9}
Bricks	1:1:1	0.81	3.7	3.37	3.72	−0.35	0.19	1.85	4.8×10^{-9}

Downloaded 06 Jul 2009 to 146.139.240.6. Redistribution subject to AIP license or copyright; see http://jap.aip.org/jap/copyright.jsp

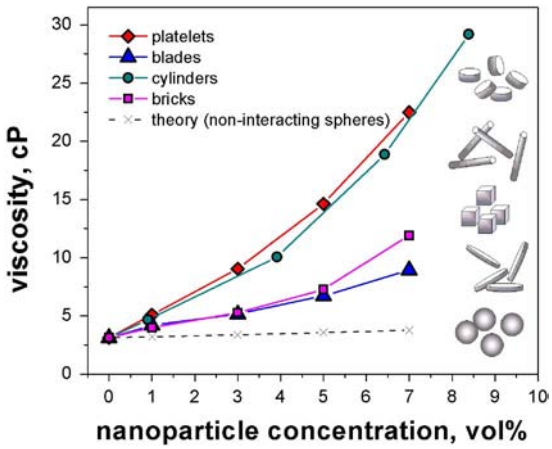

FIG. 2. (Color online) Viscosity of alumina nanofluids at 25 °C as a function of particle concentration.

that viscosity increases with particle concentration in alumina-EG/H_2O nanofluid are considerably higher than the predictions of Eq. (3) for noninteracting spheres (dashed line), indicating the strong particle-particle interactions in alumina nanofluids. Viscosity increase with increasing nanoparticle concentration in alumina nanofluids at 25 °C can be described by the following low to high sequence: blades (Dispal T25N4-80)<bricks(Catapal 200)≪cylinders(Dispal X-0)<platelets(Dispal 23N4-80). It is should be noted here that viscosity increase does not correlate with the particle shapes in the same way as thermal conductivity. Relationship between those parameters will be established in Sec. V.

Shear rate dependences for all four types of alumina nanofluids in EG/H_2O mixtures were studied in the temperature range of 15–85 °C and are summarized in Fig. 3 (viscosity at different shear rates shown by different symbols of the same color). Viscosities of suspensions with platelet and blade-shaped particles differ more than a factor of 2 [Figs. 3(a) and 3(b)] at the same particle concentration, but they both show Newtonian behavior, i.e., viscosity is independent of the shear rate. On the other hand, viscosities of nanofluids with bricklike and cylinderlike nanoparticles [Fig. 3(c) and 3(d)] at concentrations >3 vol % show shear thinning behavior: the shear viscosity decreases with increasing shear rate. As viscosity of all nanofluids decreases with increasing temperature, shear rate dependence becomes less pronounced. These results also indicate a significant impact of particle shape and aspect ratio on the rheological behavior.

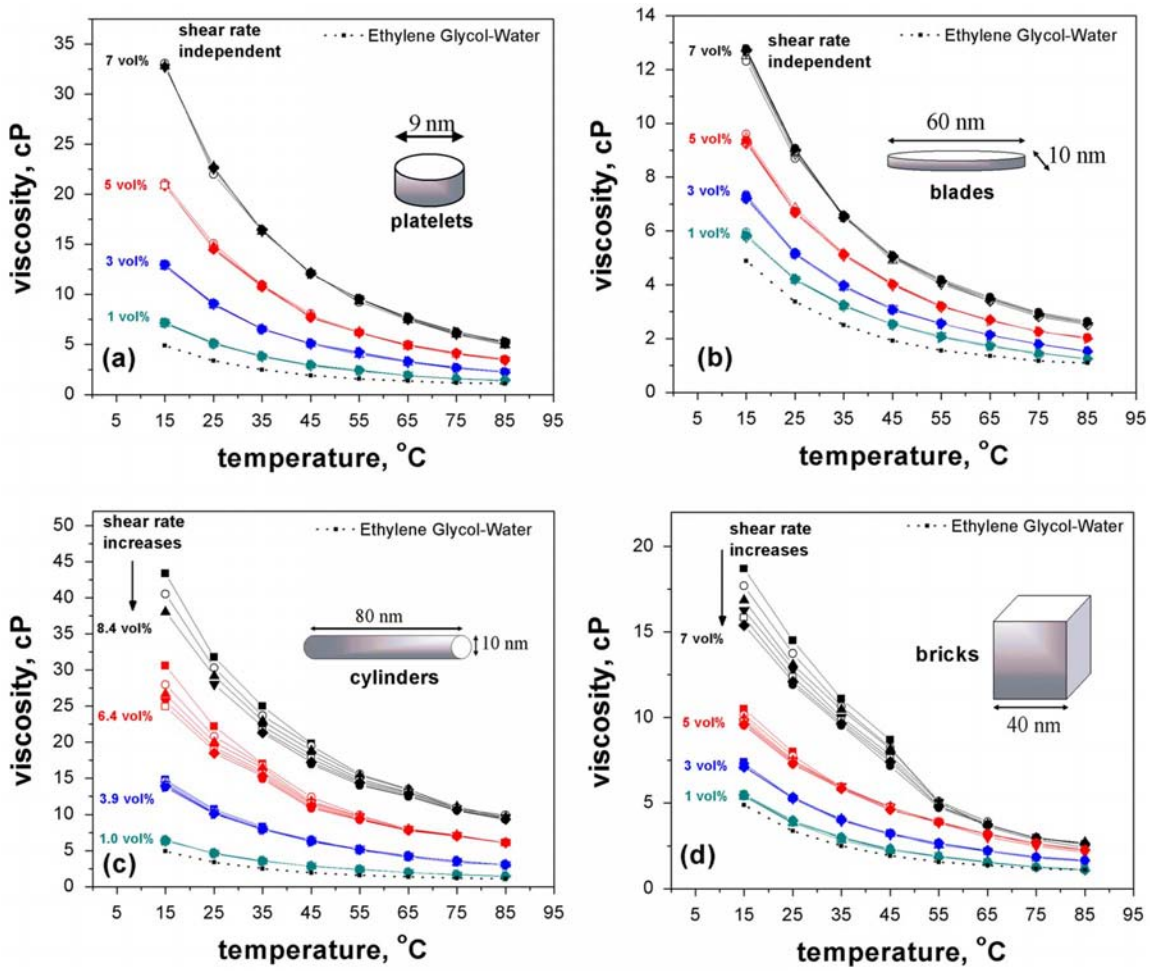

FIG. 3. (Color online) Temperature and share rate dependence of viscosity in nanofluids with different particle shapes and particle concentrations: (a) platelets, (b) blades, (c) cylinders, and (d) bricks. Viscosities at various share rates (s^{-1}) are shown by different markers: (■) 39.6, (○) 79.2, (▲) 118.8, (▼) 158.4, (□) 198.0, (♦) 237.6, and (●) 264.0.

Downloaded 06 Jul 2009 to 146.139.240.6. Redistribution subject to AIP license or copyright; see http://jap.aip.org/jap/copyright.jsp

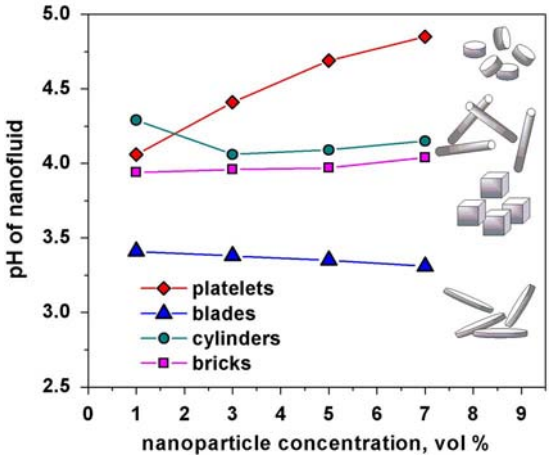

FIG. 4. (Color online) *p*H of as prepared boehmite alumina (AlOOH) in EG/H_2O suspensions.

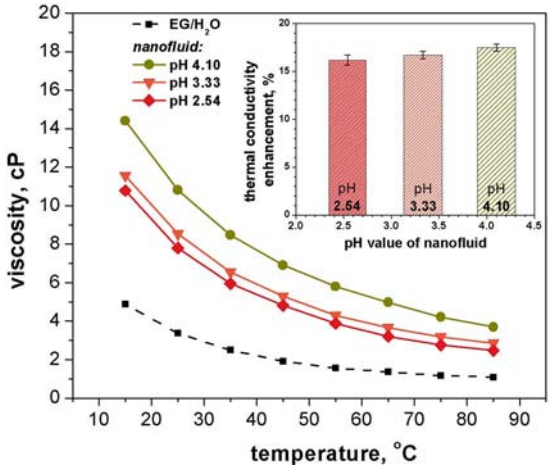

FIG. 5. (Color online) Viscosity (at shear rate of 264.0 s^{-1}) and thermal conductivity (insert) of nanofluid with 5 vol % of cylinder-shaped nanoparticles and adjusted *p*H.

D. Effect of *p*H on viscosity and thermal conductivity

To gain some knowledge about particle-fluid interactions, we measured *p*H values in stabilized alumina nanofluids. *p*H of the base fluid was 5.5. The introduction of alumina nanopowders (~1 vol %) decreases *p*H value of suspension (Fig. 4). The *p*H was independent of nanoparticle concentration except in the case of platelets where the *p*H increases with concentration. At this point it is unclear if this behavior relates to the total surface area/particle shape effects or to the presence of acid admixtures in nanopowders and will require additional studies.

In our series of nanofluids the effect of *p*H on viscosity could interfere with the particle shape effect, especially for the case of high aspect ratio nanoparticles. Nonetheless, one can see the correlation between the equilibrium *p*H and viscosity increase in alumina suspensions: nanofluids with the lowest *p*H (blades and bricks) have the lowest viscosity.

To study the effect of *p*H on viscosity and thermal conductivity and explore the potential of surface equilibria manipulation for stability and viscosity of suspensions, series of nanofluids were prepared with the same particle shape (cylinders) and volume fraction of 5 vol %. Prior to any adjustment the nanofluid's *p*H was 4.1. In two samples, *p*H was adjusted to 3.3 and 2.5 with 2*N* solution of HNO_3 in EG/H_2O. Suspensions were equilibrated for several days, and then viscosities (Fig. 5) and thermal conductivities (insert to Fig. 5) were measured. Thermal conductivity was not affected within experimental uncertainty by *p*H of suspension. On the other hand, *p*H modification from 4.1 to 3.3 resulted in viscosity drop of 25% and modification to 2.5 resulted in a total viscosity drop of 31%. The value is expressed in relation to the viscosity of initial nanofluid with *p*H 4.1 at the same temperature and was nearly independent of temperature. We also observed weaker dependence of viscosity on shear rate at lower *p*H as compared to unmodified nanofluid most likely indicating weaker interactions between nanoparticles. This is a very important result for nanofluid development showing that viscosity can be modified with almost no effect on nanofluid's thermal conductivity.

V. DISCUSSION

The absence of obvious correlation between thermal conductivity, viscosity, and the particle shape is indicative of the system's complexity. Below we analyze thermal conductivity and viscosity data with respect to the known particle shapes and other possible factors.

A. Analysis of thermal conductivity results

In this analysis we assume that in our experiments only the shape and volume fraction of nanoparticles was varied, while particle material (and thus all properties, including the value of interfacial resistance) was kept constant. For thermal conductivity analysis minor volumes of agglomerates (Table II) are treated as ensembles of individual particles separated by solid/liquid/solid interface and due to interfacial thermal resistance not contributing to thermal transfer through proposed "agglomeration mechanism."[16] Particle shapes were approximated as platelets, blades, cylinders, and bricks of certain size from the TEM images (Table I) and confirmed that they are single crystallites by XRD (Table II). Sphericity (ψ) and the shape factor (n) calculated for each adopted particle shape (Table I and III) were used in Hamilton–Crosser equation (1) to estimate thermal conductivity enhancement due to the particle shape. Results of this calculation together with experimental results are presented in Fig. 1. The predictions of Hamilton–Crosser model are higher than experimentally measured thermal conductivity, especially for blade and platelet particle shapes.

On the other hand as the sphericity decreases (shape factor increases), for the same particle volume fraction, the total surface area of solid/liquid interface also increases. If we assume that contribution of interfacial effects to thermal conductivity is proportional to total area of the interface, we can estimate the value of Kapitza resistance and Kapitza length from our experimental data because varying the shape and size of nanoparticles also varies the total surface area of the solid/liquid interface.

Thus if both the value of surface heat resistance and surface area of solid-liquid interface are high, the thermal

Downloaded 06 Jul 2009 to 146.139.240.6. Redistribution subject to AIP license or copyright; see http://jap.aip.org/jap/copyright.jsp

conductivity enhancement due to the particle shape will be diminished by negative contribution of interfacial effects. Assuming linearity of both, particle shape and interfacial contributions with particle volume fraction, thermal conductivity of nanoparticle suspension can be presented as follows:

$$\frac{k_{\text{eff}}}{k_0} = 1 + (C_k^{\text{shape}} + C_k^{\text{surface}}) \quad , \tag{6}$$

where C_k^{shape} and C_k^{surface} are coefficients reflecting contributions to the effective thermal conductivity due to particle shape (positive) and due to surface resistance (negative) correspondingly. Particle shape coefficient C_k^{shape} is described by Hamilton–Crosser equation and calculated for our particle shapes in Table III. Experimental slopes C_k (Fig. 1) are significantly lower than predicted from C_k^{shape} alone due to the negative contribution of the interfacial resistance C_k^{surface}. Physical deductions would assume that the contribution of interfacial effects should be proportional not only to the volume fraction but also to the surface area of nanoparticles. Here we introduce a surface factor f representing surface area of nanoparticles normalized per unit volume and defined as ratio between the surface and the volume for the particle of certain shape and size (Table III). According to the definition of interfacial Kapitza resistance equation (2), physical meaning of negative interfacial contribution to the total thermal conductivity C_k^{surface} would be the volume of base fluid excluded from the heat transfer process due to surface resistance. The latter can be approximated as follows:

$$C_k^{\text{surface}} = -f \cdot l_k. \tag{7}$$

Expressions (1), (2), (6), and (7) allow us to calculate the Kapitza length l_k and interfacial Kapitza resistance R_k from our experimental thermal conductivity data, which are unique resistance characteristics of a particular surface-liquid interface. Despite some assumptions and approximate particle sizes, chosen for modeling, one can see (Table III) good consistency for all particle shapes in the values of the Kapitza length averaged to 1.61 nm for boehmite alumina-EG/H_2O interface and interfacial surface resistance is averaged at 4.35×10^{-9} m^2 K/W, which is within lower range of R_k reported for nanofluids.[9,19] This justifies the assumption of using nominal, nonaggregated particle shape/sizes for thermal conductivity analysis.

The thermal conductivity model accounting for both particle shape and interfacial contributions proportional to the total surface area of nanoparticles is illustrated in Fig. 6. Due to particle shape effect, described by Hamilton–Crosser equation (1), thermal conductivity of suspension (5 vol % used in this calculation) increases as sphericity of nanoparticles decreases (solid line). However, the negative contribution of interfacial effect (dash line), proportional to Kapitza length (average value of l_k used) and the total surface area of nanoparticles, compensates for the increase. One can see that when the sphericity of nanoparticles is below 0.6 (shape factor of 5) the negative contribution of the interfacial effects increases much faster than the particle shape contribution. Thus, overall thermal conductivity of suspension (dash-dot line) starts decreasing below sphericity of 0.6.

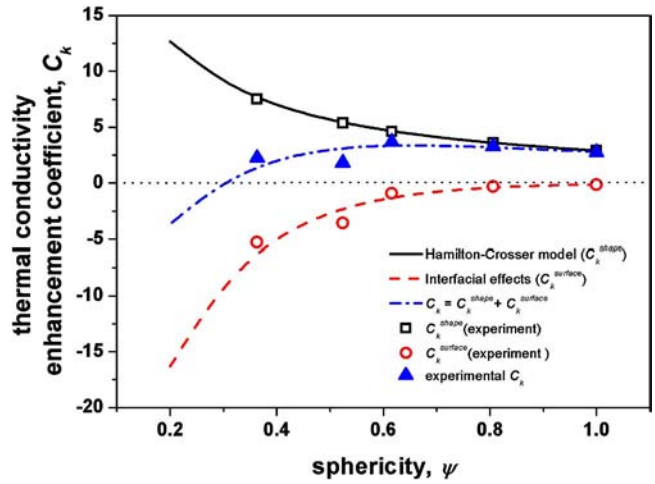

FIG. 6. (Color online) Contribution of particle shape effect (Hamilton Crosser model) and interfacial thermal resistance to the thermal conductivity of nanoparticle suspension (5 vol %) at various particle sphericities.

B. Analysis of rheological properties

From results presented in Fig. 2, one can see that viscosities of alumina nanofluids at <0.1 increase nonlinearly with nanoparticle concentration, much faster than predicted by Einstein–Batchelor formula for spherical noninteracting particles.[25] Failure of traditional viscosity theories to adequately describe experimental results for nanofluids even with low particle concentration (<0.1) have been reported in the literature[31–37] and considered as an indicator of particle-particle interactions, structural limitations due to the presence of high aspect ratio particles and agglomerates, or increased effective particle volumes since some liquids are immobilized between particles or combination of both.

Molecular dynamic simulation[38] showed that effective viscosity of nanoparticle suspensions ($_{\text{eff}}$) is proportional to the volume concentration of dispersed nanoparticles and can be described as

$$_{\text{eff}}(\ ) = \ _0(1 + A_1 \ + A_2 \ ^2), \tag{8}$$

where $_0$ is the viscosity of the base fluid and A_1 and A_2 are constants. Our experimental data were fitted by this equation and coefficients A_1 and A_2 for the room-temperature viscosity are presented in Table IV. Experimental values of A_1 and A_2 are significantly higher than coefficients in Einstein–Batchelor equation for spherical noninteracting particles. It also should be noted here that A_2 and A_1 coefficients vary significantly with particle shape. The highest viscosity increase was observed in nanofluids with plateletlike nanoparticles and A_1, A_2 coefficients agree well with the results on gamma-alumina/water nanofluid reported in Ref. 34 that calculated $A_1 = 39.1$ and $A_2 = 533.9$ for nanofluids with up to

TABLE IV. Viscosity enhancement coefficients at 25 °C: $_{\text{eff}}(\ ) = \ _0(1+A_1 \ +A_2 \ ^2)$.

	Platelets	Blades	Cylinders	Bricks
A_1	37.1	14.6	13.5	1.9
A_2	612.6	123.3	904.4	471.4

Downloaded 06 Jul 2009 to 146.139.240.6. Redistribution subject to AIP license or copyright; see http://jap.aip.org/jap/copyright.jsp

10 vol % of solids (particle size of 13 nm, spheres).[34]

As we mentioned earlier the viscosity increase with vol % of nanoparticles correlates with suspension *p*H: the highest viscosity increase was observed in nanofluid with the highest *p*H in the series. Alumina is amphoteric oxide and chemical equilibria in the alumina suspension involve exchange of ions (H+ or OH-) between particle surface and bulk fluid, establishing surface charge, degree of particle-particle interactions, and *p*H of bulk suspension. Isoelectric point (*p*H at which charge at the surface is zero) for boehmite alumina is 9–10.[24] The further the solution *p*H from this value, the higher is the charge at the particle surface. Increased repulsion between the particles of the same charge results in weaker particle-particle interactions and thus lower viscosity. This finding was confirmed in a separate experiment with *p*H adjustment and was consistent with the concept of surface charge increasing as nanofluid's *p*H gets further from the isoelectric point. This approach in viscosity modification, however, has a limitation on practical (corrosion) and theoretical sides. Derjaguin-Landau-Verwey-Overbeek (DLVO) theory[25] predicts that as charge separation in double electric layer increases, shrinkage of double layer occurs (Debye length $\rightarrow 0$) and at small separations between nanoparticles the van der Waals attraction wins over the double layer repulsion and particle agglomeration occurs (observed as a viscosity increase). This scenario, however, is out of the range of *p*H values we have studied since viscosity was only decreasing as we shifted *p*H further from isoelectric point.

The isoelectric point is temperature dependent and shifts toward lower *p*H values as temperature increases.[39] Thus at given *p*H, surface charge decreases with the temperature increase which might result in particle agglomeration and drastic viscosity increase. Accounting for logarithmic nature of *p*H scale, the knowledge of suspension's *p*H with respect to isoelectric point for nanoparticle material must be considered for commercial applications of nanofluids at elevated temperatures.

Besides critical role of surface charges in nanoparticle agglomeration and viscosity, particle shape effect might also play a role in abnormally increased viscosity of alumina nanofluids. Shear rate dependence of viscosity in cylinder and bricklike nanoparticle suspensions indicates some restriction in fluid movement due to particle alignment and/or agglomeration. In a steady state, a rodlike particle or elongated agglomerate[22] can have two types of motion due to the Brownian movements: rotational (end-over-end) motion around the midpoint and translational motion in parallel or perpendicular to the long axis. When the average spacing between particles is much larger than the longest dimension of the particle, the rotational and translational motions are not restricted by each other; hence very weak shear thinning behavior is expected. In suspension with cylinders (aspect ratio $p=8$; defined as $p=L/d$, where L and d are the length and diameter of the particles), free motion of particles is possible when the number density (c) is between 0 and $1/L^3$ that corresponds to the volume fraction between 0 and $1/p^2$ ($0< \quad <0.0156$). In suspensions of cylinders with higher volume fractions ($>1.56\%$) nanoparticles start to interact, so

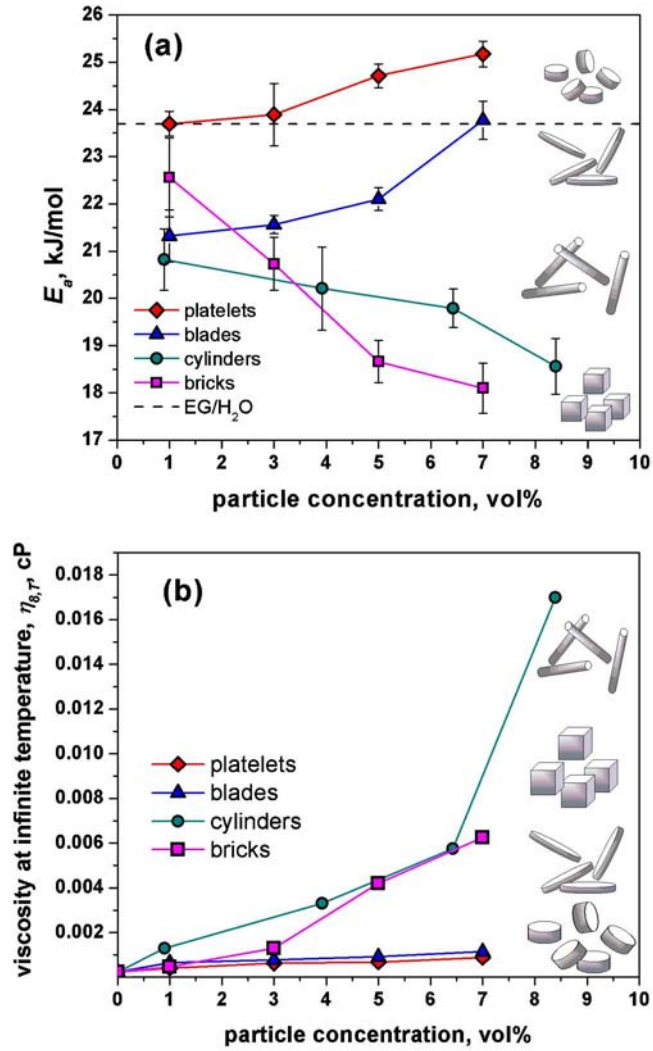

FIG. 7. (Color online) Analysis of experimental data on nanofluid's viscosity by Arrhenius type equation: (a) E_a (activation energy to fluid flow) as a function of particle concentration in nanofluid with various particle shapes and (b) $_{\infty,T}$ (viscosity at "infinite" temperature).

the viscosities at zero shear rate can be much greater than the base fluid viscosity and be very sensitive to the shear.

Because of the statistics of random clustering, nanoparticle agglomerates are usually elongated[22] and behave similar to high aspect ratio particles, restricting both rotational and translational motions. This results in shear thinning behavior and higher viscosities of suspensions with agglomerates. Shear thinning behavior was observed not only in suspensions of cylinderlike nanoparticles but also in suspension bricklike particles, which according to DLS spectra contain <25 vol % of low aspect ratio particles agglomerated into 220 nm clusters (Table II).

Temperature dependence of nanofluids viscosity (Fig. 3) was analyzed using logarithmic form of Arrhenius, Eq. (4), and flow parameters E_a and $_{\infty,T}$ were calculated for different particle concentrations (Fig. 7) within temperature range of 15–55 °C. In studied particle concentration range, E_a of alumina nanofluids with blade, cylinder, and brick-shaped particles are below that for base fluid [Fig. 7(a)], while suspension of plateletlike nanoparticles has higher E_a values. Thus,

Downloaded 06 Jul 2009 to 146.139.240.6. Redistribution subject to AIP license or copyright; see http://jap.aip.org/jap/copyright.jsp

it appears that addition of nanoparticles to EG/H_2O may affect activation energy for viscous flow in different ways.

Physical interpretation of activation energy of viscous flow (E_a) has not been developed for nanoparticle suspensions. Generally, the activation energy is the energy barrier, which must be overcome, in order for the fluid layers to move past each other. A large E_a means it is more difficult for the fluid layers to move past each other. In fluids the activation energy reflects attraction forces between molecules of the fluid.[40] By analogy in nanofluids E_a values should still reflect adhesion forces between molecules of base fluid but their interactions are modified due to the presence of nanoparticles. Interpretation of E_a, however, must be considered in combination with the values of pre-exponential factor $_{\infty,T}$.

At infinite temperature kinetic energy of nanoparticles is very high and particle interactions that contribute to viscosity at room temperature are no longer effective. At this point the viscosity is governed purely by the geometric structure of the nanofluid. So the value of $_{\infty,T}$ is representative of a structural contribution of the nanoparticles to the viscosity. Figure 7(b) illustrates that the introduction of nanoparticles always raises structural constraints to the fluid flow, especially in the case of elongated (cylinders) and slightly agglomerated (bricks) particle suspensions. The presence of significant structural constraints for those two nanofluids is also observed in shear rate dependence of viscosity at low temperatures.

In many applications coolant's behavior at elevated temperatures is most important. Deduced from Fig. 3, viscosity of nanofluids decreases slower with the temperature than viscosity of base fluid. The less structural constraints in base fluid make it easier for base fluid to flow as kinetic energy rises, while in nanofluids particles resist moving with the fluid molecules.

C. Evaluation of efficiency of nanofluids

Effectiveness of various liquid coolants depends on the flow mode (laminar/turbulent) can be estimated based on fluid dynamics equations. According to Ref. 5, in the simple case of fully developed laminar flow, use of nanofluid will be beneficial if the increase in the viscosity is less than four times of the increase in thermal conductivity,[5]

$$\frac{\ _{\text{eff}}}{\ _0} \approx 1 + C \quad , \quad \frac{k_{\text{eff}}}{k_0} = 1 + C_k \quad , \quad C\ /C_k < 4, \tag{9}$$

where C and C_k are viscosity and thermal conductivity enhancement coefficients, determined from experimental viscosity and thermal conductivity ratios.

Examination of experimental data by this criterion is presented in Table V. As prepared all alumina nanofluids have viscosity increases higher than four times the thermal conductivity increase, meaning that despite higher thermal conductivities, efficiencies of these nanofluids will be low due to higher pumping power required. We also showed in our experiments that adjusting surface charge at nanoparticles in suspension could alter viscosity without affecting the thermal conductivity. This improves the thermal conductivity/viscosity enhancement ratio, but even in modified alumina nanofluids penalty for introduction of nanoparticles due to increased pressure drop is still too high according to this criterion for laminar flow mode.

TABLE V. Evaluation of nanofluid performance in laminar and turbulent flow regime.

		Laminar flow	Turbulent flow	
	vol %	$C\ /C_k$	$\text{Mo} = \frac{\rho^{0.8}k^{0.67}c_p^{0.33}}{\ _{0.47}}$	Performance, % of base fluid
EG-H_2O	50/50		4.51	0.0
Platelets Dispal 23N4-80	1	19.9	3.79	−15.8
	3	21.8	3.03	−32.8
	5	31.8	2.53	−43.9
	7	65.5	2.17	−51.9
Blades Dispal T25N4-80	1	7.7	4.18	−7.3
	3	8.0	3.95	−12.3
	5	9.9	3.64	−19.2
	7	11.7	3.34	−25.9
Cylinders Dispal X-0	1	20.5	3.98	−11.7
	3.9	26.1	3.05	−32.2
	6.4	31.6	2.44	−45.9
	8.4	35.9	2.11	−53.2
Bricks Catapal 200	1	5.0	4.28	−5.1
	3	5.0	3.97	−12.0
	4	6.5	3.60	−20.1
	5	9.8	3.02	−32.9

For turbulent flow mode the Mouromtseff (Mo) value was suggested as a figure of merit for comparing the heat transfer capabilities of various coolants.[41] For turbulent flow the heat transfer rate is dependent not only on k but also on the other thermophysical properties of the fluid,

$$\text{Mo} = \frac{\rho^{0.8}k^{0.67}c_p^{0.33}}{\ _{0.47}}, \tag{10}$$

where ρ, k, c_p, and represent the density, thermal conductivity, specific heat (at constant pressure), and dynamic viscosity of the fluid. The significance of the Mouromtseff value lies in the fact that for flow over or through a given geometry at a specified velocity, the liquid coolant with the largest Mouromtseff value will provide the highest heat transfer rate. Table V compares the efficiencies of alumina nanofluids in turbulent flow at 25 °C using Mouromtseff values and also compares these parameters to the base fluid characteristics. In turbulent regime performance of nanofluids also strongly depends on viscosity. Nanofluids with reasonably low viscosity (bladelike and bricklike nanoparticles) offer better performance than nanofluids with highest thermal conductivity and high viscosity (cylinderlike nanoparticles). However, overall cooling performance of alumina nanofluids is 5%–53% worse than the base fluid: very high viscosity degrades the effect of higher thermal conductivity. Lowering the viscosity of alumina nanofluids by pH adjustment or an-

Downloaded 06 Jul 2009 to 146.139.240.6. Redistribution subject to AIP license or copyright; see http://jap.aip.org/jap/copyright.jsp

other technique could improve nanofluid performance. This result confirms that in characterization of nanofluids thermal conductivity cannot be considered alone as a criterion for nanofluid selection. Viscosity of nanofluids is important as well, and sometimes nanofluids with lower thermal conductivity enhancements may be preferred because of lower viscosities.

VI. CONCLUSIONS

Studies of particle shape effect on thermophysical properties of alumina-EG/H_2O suspensions are reported. Our investigation points out the significance of complex interaction between nanoparticles and base fluids in determining the thermal conductivity and viscosity enhancements. In nanofluids with nonspherical particles, thermal conductivity enhancements predicted by Hamilton–Crosser equation are diminished by negative contribution of heat flow resistance at the solid-liquid interface. Using EMT and the assumption that contribution of interfacial effects is proportional to the total surface area of nanoparticles (changes with the shape and size), we obtained consistent value of Kapitza resistance from our experimental data. The model showed that for EG/H_2O suspensions of nonspherical alumina particles studied in this paper, overall thermal conductivity starts decreasing below sphericity of 0.6.

Viscosities of nanofluids were shown to depend on both particle shapes and surface properties of nanoparticles. Elongated particles and agglomerates result in higher viscosity at the same volume fraction due to structural limitation of rotational and transitional Brownian motions. For lower viscosities spherical particles or lower aspect ratio spheroids should be used. Surface charge at nanoparticles influences particle/base fluid interactions and agglomeration of individual nanoparticles. We demonstrated that viscosity of the alumina-based nanofluids might be decreased by 31% without affecting thermal conductivity by adjusting surface charge with *p*H of suspension.

It was also demonstrated that evaluation of nanofluids for a particular application requires a proper understanding of all the characteristics and thermophysical properties of nanoparticle suspensions. Use of alumina nanofluids investigated in this paper would not be beneficial in laminar or turbulent flow mode, unless viscosity is decreased.

ACKNOWLEDGMENTS

We are grateful to Sasol North America Inc. for providing the nanoparticle samples of boehmite alumina used in this study. This work was sponsored by the U.S. Department of Energy's Office of Vehicle Technologies, under Contract No. DE-AC02-06CH11357 at Argonne National Laboratory, managed by the University of Chicago Argonne LLC (USA). This work was also supported by U.S. Army REECOM-TARDEC under a "Work for Others" Contract No. P-08071.

[1]S. Kabelac and J. F. Kuhnke, Annals of the Assembly for International Heat Transfer Conference, 2006, Vol. 13, p. KN-11.
[2]V. Trisaksri and S. Wongwises, Renewable Sustainable Energy Rev. **11**, 512 (2007).
[3]W. H. Yu, D. M. France, J. L. Routbort, and S. U. S. Choi, Heat Transfer Eng. **29**, 432 (2008).
[4]S. C. Mohapatra, http://electronics-cooling.com/articles/2006/2006_may_a2.php.
[5]R. Prasher, D. Song, J. L. Wang, and P. Phelan, Appl. Phys. Lett. **89**, 133108 (2006).
[6]S. M. S. Murshed, K. C. Leong, and C. Yang, Int. J. Therm. Sci. **47**, 560 (2008).
[7]J. C. Maxwell, *Electricity and Magnetism* (Clarendon, Oxford, 1873).
[8]R. L. Hamilton and O. K. Crosser, Ind. Eng. Chem. Fundam. **1**, 187 (1962).
[9]C. W. Nan, R. Birringer, D. R. Clarke, and H. Gleiter, J. Appl. Phys. **81**, 6692 (1997).
[10]O. M. Wilson, X. Y. Hu, D. G. Cahill, and P. V. Braun, Phys. Rev. B **66**, 224301 (2002).
[11]J. L. Barrat and F. Chiaruttini, Mol. Phys. **101**, 1605 (2003).
[12]W. Yu and S. U. S. Choi, J. Nanopart. Res. **5**, 167 (2003).
[13]H. Q. Xie, M. Fujii, and X. Zhang, Int. J. Heat Mass Transfer **48**, 2926 (2005).
[14]H. Q. Xie, J. C. Wang, T. G. Xi, Y. Liu, F. Ai, and Q. R. Wu, J. Appl. Phys. **91**, 4568 (2002).
[15]B. X. Wang, L. P. Zhou, and X. F. Peng, Int. J. Heat Mass Transfer **46**, 2665 (2003).
[16]R. Prasher, W. Evans, P. Meakin, J. Fish, P. Phelan, and P. Keblinski, Appl. Phys. Lett. **89**, 143119 (2006).
[17]R. Prasher, P. Bhattacharya, and P. E. Phelan, Trans. ASME, Ser. C: J. Heat Transfer **128**, 588 (2006).
[18]S. P. Jang and S. U. S. Choi, Appl. Phys. Lett. **84**, 4316 (2004).
[19]R. Prasher, P. Bhattacharya, and P. E. Phelan, Phys. Rev. Lett. **94**, 025901 (2005).
[20]M. P. Beck, T. F. Sun, and A. S. Teja, Fluid Phase Equilib. **260**, 275 (2007).
[21]J. Eapen, W. C. Williams, J. Buongiorno, L. W. Hu, S. Yip, R. Rusconi, and R. Piazza, Phys. Rev. Lett. **99**, 095901 (2007).
[22]E. V. Timofeeva, A. N. Gavrilov, J. M. McCloskey, Y. V. Tolmachev, S. Sprunt, L. M. Lopatina, and J. V. Selinger, Phys. Rev. E **76**, 061203 (2007).
[23]D. G. Cahill, W. K. Ford, K. E. Goodson, G. D. Mahan, A. Majumdar, H. J. Maris, R. Merlin, and S. R. Phillpot, J. Appl. Phys. **93**, 793 (2003).
[24]*The Environmental Chemistry of Aluminum*, edited by G. Sposito (CRC, Lewis, Boca Raton, FL, 1996).
[25]R. D. Vold and M. J. Vold, *Colloid and Interface Chemistry* (Addison-Wesley, Reading, MA, 1983).
[26]R. G. Larson, *The Structure and Rheology of Complex Fluids* (Oxford University Press, New York, 1999).
[27]S. L. Phillips and D. L. Perry, *Properties of Inorganic Compounds* (CRC, Boca Raton, FL, 2000).
[28]Q. Li and Y. Xuan, Chin. J. Sci. Instrum. **26**, 678 (2005).
[29]B. D. Cullity and S. R. Stock, *Elements of X-Ray Diffraction*, 3rd ed. (Prentice Hall, Englewood Cliffs, NJ, 2001).
[30]D. Cookson, N. Kirby, R. Knott, M. Lee, and D. Schultz, J. Synchrotron Radiat. **13**, 440 (2006).
[31]J. Buongiorno, Trans. ASME, Ser. C: J. Heat Transfer **128**, 240 (2006).
[32]X. W. Wang, X. F. Xu, and S. U. S. Choi, J. Thermophys. Heat Transfer **13**, 474 (1999).
[33]K. Kwak and C. Kim, Korea-Aust. Rheol. J. **17**, 35 (2005).
[34]B. C. Pak and Y. I. Cho, Exp. Heat Transfer **11**, 151 (1998).
[35]S. E. B. Maiga, C. T. Nguyen, N. Galanis, and G. Roy, Superlattices Microstruct. **35**, 543 (2004).
[36]S. Lee, S. U. S. Choi, S. Li, and J. A. Eastman, Trans. ASME, Ser. C: J. Heat Transfer **121**, 280 (1999).
[37]J.-H. Lee, K. S. Hwang, S. P. Jang, B. H. Lee, K. H. Kim, S. U. S. Choi, and C. J. Choi, Int. J. Heat Mass Transfer **51**, 2651 (2008).
[38]V. Y. Rudyak, A. A. Belkin, E. A. Tomilina, and V. V. Egorov, Defect Diffus. Forum **273–276**, 566 (2008).
[39]A. López Valdivieso, J. L. Reyes Bahena, S. Song, and R. Herrera Urbina, J. Colloid Interface Sci. **298**, 1 (2006).
[40]S. Morioka, X. F. Bian, and M. H. Sun, Z. Metallkd. **93**, 288 (2002).
[41]R. E. Simons, http://electronics-cooling.com/articles/2006/ 2006_may_c-c.php.

Downloaded 06 Jul 2009 to 146.139.240.6. Redistribution subject to AIP license or copyright; see http://jap.aip.org/jap/copyright.jsp